An Embedded Boundary Integral Solver for the Unsteady Incompressible Navier-Stokes Equations[1]

George Biros∗, Lexing Ying∗,and Denis Zorin∗
∗ *Courant Institute of Mathematical Sciences, New York University, New York 10012*
Email: {biros,lexing,dzorin}@cs.nyu.edu

Version: November 2002

We present a new method for the solution of the unsteady incompressible Navier-Stokes equations. Our goal is to achieve a robust and scalable methodology for two and three dimensional incompressible laminar flows. The Navier-Stokes operator discretization is done using boundary integrals and structured-grid finite elements. We use a two-step second-order accurate scheme to advance the equations in time. The convective term is discretized by an explicit, but unconditionally stable, semi-Lagrangian formulation; at each time step we inverta spatial constant-coefficient (modified) Stokes operator. The Dirichlet problem for the modified Stokes operator is formulated as a double-layer boundary integral equation. Domain integrals are computed via finite elements with appropriate forcing singularities to account for the irregular geometry. We use a velocity-pressure formulation which we discretize with bilinear elements (Q1-Q1), which give equal order interpolation for the velocities and pressures. Stabilization is used to circumvent the div-stability condition for the pressure space. The integral equations are discretized by Nyström's method. For the specific approximation choices the method is second order accurate. We will present numerical results and discuss the performance and scalability of the method in two dimensions.

Key Words: Stokes equations, integral equations, double-layer potential, fast multipole methods, embedded domain methods, immersed interface methods, fictitious domain methods, Cartesian grid methods, moving boundaries

1. INTRODUCTION

In [3] we have introduced the Embedded Boundary Integral method (EBI) for the steady Stokes equations. In this article we extend this method to the incompressible Navier-Stokes equations.

Our ultimate goal is to develop algorithms for viscous flows with moving boundaries that discretize the fluid equations on static grids to avoid the high costs of time-dependent mesh generation.

Our method relies on the idea proposed in A. Mayo's work [15] which combines a boundary integral formulation with fast solvers on a regular volume grid. The boundary integral formulation is attractive for simulation of fluids with dynamic boundaries because it allows for natural coupling of the equations for the fluid and surrounding or immersed solids.

Pure boundary integral formulation can be used for certain types for PDEs. This approach eliminates the need for meshing of the volume and it reduces the size of the discrete problem decreasing the problem dimension by one. Although Navier-Stokes equations do

[1]This work is supported by the National Science Foundation's Knowledge and Distributed Intelligence (KDI) program through grant DMS-9980069.

not admit a boundary integral formulation directly, most effective methods to solve the Navier-Stokes equations involve linearizations, and thus integral equations can be used. There are a number of difficulties with a pure boundary integral formulation. The linearization of the convective term results in linear PDEs with non-constant coefficients; for such equations the construction of the fundamental solution is as difficult as solving the original problem. Furthermore, distributed volume forces are present in the equations. Computing integrals for such volume terms, also known as *Newton potentials*, requires acceleration methods such as Fast multipole methods (FMM), [7]. Another important problem is that the integrals are difficult to evaluate accurately for points close to the boundary because the kernels become nearly singular. Accurate and fast integration schemes are yet to be found in three dimensions.

The EBI method replaces explicit integral evaluations with solving the equations on a simpler domain. With EBI method we embed the flow domain inside a larger domain, for which fast-scalable solvers are available (we use a regular grid) and to which the velocity and pressure fields are extended. We use an integral formulation to compute the interface jumps of the velocity and its derivatives and then we use Taylor expansions to express these jumps as a source term at regular grid points close to the interface. This source term, which appears in the right hand side of a the regular grid problem, we call Taylor Expansion Stencil Correction (TESC). Depending on the details of the implementation, the method can be first, second, or higher order accurate. EBI originally appeared in Anita Mayo's work [15] for the Laplace and biharmonic operators. The details of this method and its application to the steady Stokes problem are described in [3]. We should mention that using regular grids is not the best approach for high Reynolds numbers due to the presence of thin boundary layers. A block structured grid has to be used in in this case; however, overall structure of the method can be preserved. In this paper we consider only regular grids.

The basic components of the embedded boundary integral method, outlined in Section 2 are a Cartesian grid solver for the modified Stokes equations and a boundary integral solver for the homogeneous modified Stokes equations. In order to extend EBI method to the Navier-Stokes we need two new tools: a semi-Lagrangian formulation for the convective term, and a double layer formulation for the *modified* Stokes operator

$$\alpha \boldsymbol{u} - \nu \Delta \boldsymbol{u} + \nabla p = 0, \quad \operatorname{div} \boldsymbol{u} = 0.$$

described in Sections 4 and 3 respectively.

Related work. For each of the three principal aspects of the method (boundary integral equations, Cartesian grid solvers, semi-Lagrangian methods) there is a substantial body of work which we discuss briefly in relation to our method.

Integral equation formulations for the Navier-Stokes equations. There have been several attempts to use boundary integral equations to solve the steady and unsteady incompressible Navier-Stokes equations. The majority of algorithms are based on non-primitive variable formulations, for example, velocity-vorticity and stream function vorticity formulations. The latter, combined with a Lagrangian treatment of the convective method, are also known as vortex methods. Here we do not attempt a comprehensive review of the literature but we have chosen some representative articles.

In [6] a stream function formulation is used to solve the steady- and unsteady-state Navier-Stokes equations. The steady-state one is solved by using a volume potential approximation for the stream function in combination with a Newton method or a fixed point

method. The volume integrals are carried out by solving non-homogeneous Poisson problems on the disk; thus each GMRES iteration for the Newton step requires two Poisson solves and one homogeneous biharmonic solve. The unsteady case uses a similar approach but the convective terms are treated explicitly.

Integral equations are used in [2], with a stream function-vorticity formulation. Integral equations are used to compute the correct boundary condition for the vorticity and then a mortar-type unstructured grid finite element method is used to solve elliptic problems for the vorticity and stream functions. This method requires four scalar regular grid solves and one boundary integral solve.

In [18] a velocity-vorticity formulation is used. A Lagrangian approach is coupled with an explicit diffusion step to advance the vorticity. Volume integrals are used to compute the voriticity that corresponds to non-slip boundary conditions around a sphere. The method is combined with fast parallel multipole methods and is shown to resolve the flow for high Reynolds numbers.

In contrast to these methods, we chose to use the primitive variable formulation (velocity and pressure). We intend to use our method as a building block for fluid-solid interaction problems; in this case the interface conditions often include both Neumann and Dirichlet conditions, and such conditions are best treated using primitive variables.

Existing velocity-pressure formulations using boundary integral equations are based on the explicit treatment of the convective term. As we have mentioned, the problem with this approach is the need to compute the Newton potentials accurately enough to resolve the boundary layer. A popular method is the Dual Reciprocity Method [19] in which a radial basis function interpolant of the convective term is constructed. There are several open issues with this approach: the optimal choice of the interpolation scheme, the number of interpolation basis functions and its considerable computational cost. Moreover, although several researchers have attempted to use it to solve viscous flow problems, the results are appear to be unsatisfactory.

Cartesian grids. There is an extensive literature on solving Navier-Stokes equations on regular grids. We discuss briefly some of the papers most closely related to our work.

In [14] the immersed interface method is used to solve Navier-Stokes equations with elastic boundaries approximated by spring systems. Dirichlet problems can be solved by using very stiff springs; the jumps come from explicit time stepping on the boundary deformation.In [13] the immersed boundary method is used to compute a flow around the cylinder. Dirichlet conditions are also applied approximately by using very stiff springs. The time restriction from the explicit coupling of the springs and the flow is quite severe, requiring two orders of magnitude smaller a time step than that dictated by accuracy considerations.

In [4] the Navier-Stokes equations are used with a stream function-vorticity formulation, using the immersed interface method. Time stepping is done through a fractional step approach in which the convective terms are treated explicitly and thus a CFL-type restriction applies. The diffusive terms are solved with the immersed interface method. Additional equations are used for the interface conditions and Schur complement matrix is computed and then factored in order to make the computation efficient.

Semi-Lagrangian methods. The Semi-Lagrangian methods (which are also known as Lagrange-Galerkin, spline-characteristic method, or characteristic-Galerkin) allow for explicit, yet stable treatment of convection. The time derivative is discretized in Lagrangian framework, however unlike Lagrangian methods that track particles through time and need

regridding, the particles are traced back from the grid points. This processes is repeated at every time step and it requires the solution of a ODE (backward in time) and an a interpolation scheme to compute the past velocity at the departure points. The latter is the biggest source of complications since it can introduce excessive diffusion. In some sense, semi-Lagrangian methods can be viewed as a very effective upwind schemes. In [5], the method is used for convection-diffusion equations and in [17] for the Navier-Stokes equations. A good review for structured grids is given in [20]. For unstructured grids, spectral methods and more complete references on semi-Lagrangian methods see [22].

Notation. Scalars will be denoted with lowercase italics, vectors with lowercase boldface letters; tensors and matrices will be denoted with uppercase boldface letters. Infinitely dimensional quantities will be in italics, whereas finite dimensional ones (usually discretizations) will be non-italic fonts.

2. DESCRIPTION OF THE EMBEDDED BOUNDARY INTEGRAL METHOD

We seek solutions of the incompressible Navier-Stokes equations in a multiply connected domain with Dirichlet boundary conditions. We choose a primitive variable formulation (velocities and pressures), for which the momentum and mass conservation laws are given by

$$\begin{aligned} \frac{\partial \boldsymbol{u}}{\partial t} + (\nabla \boldsymbol{u})\boldsymbol{u} - \nu \Delta \boldsymbol{u} + \nabla p = \boldsymbol{0}, \quad \text{in} \quad \omega \times (0,T], \\ \operatorname{div} \boldsymbol{u} = \boldsymbol{0}, \quad \text{in} \quad \omega \times [0,T], \\ \boldsymbol{u} = \boldsymbol{g}, \quad \text{on} \quad \gamma \times (0,T], \quad \boldsymbol{u}(\omega,0) = \boldsymbol{u}_{init}. \end{aligned} \tag{1}$$

Here $\boldsymbol{u}$ is the velocity field, p is the pressure, and $\boldsymbol{g}$ is a given Dirichlet boundary condition for the velocity.

The above equation can be solved by a semi-implicit time stepping in which the convective term is lagged. For example for a backward Euler method at each time step we use the old values of velocity $\boldsymbol{u}_0$ to solve for the new velocity and pressure $\boldsymbol{u}$, p:

$$\frac{\boldsymbol{u}}{\delta t} - \nu \Delta \boldsymbol{u} + \nabla p = \frac{\boldsymbol{u}_0}{\delta t} - (\nabla \boldsymbol{u}_0)\boldsymbol{u}_0 \qquad \operatorname{div} \boldsymbol{u} = \boldsymbol{0}, \quad \text{in} \quad \omega. \tag{2}$$

At every time step a system of the following general form must be solved:

$$\alpha \boldsymbol{u} - \nu \Delta \boldsymbol{u} + \nabla p = \boldsymbol{b}, \quad \text{in} \quad \omega \qquad \operatorname{div} \boldsymbol{u} = \boldsymbol{0}, \quad \text{in} \quad \omega, \qquad \boldsymbol{u} = \boldsymbol{g}, \quad \text{on} \quad \gamma. \tag{3}$$

Here α depends on the time-stepping scheme and $\boldsymbol{b}$ includes the terms that carry information on the history of the flow. In order to avoid CFL-related time restrictions we use a semi-Lagrangian approach (4).

We split the solution of the problem into several steps as follows. We first embed ω in an easy-to-discretize domain Ω; we use a rectangle, but other domains can be used. By linearity we decompose (3) into two problems: a problem with an inhomogeneous body force and zero boundary conditions for Ω, and a problem with no body force, but nontrivial boundary conditions:

$$\alpha \boldsymbol{u}_1 - \nu \Delta \boldsymbol{u}_1 + \nabla p_1 = \boldsymbol{b} \quad \text{in} \quad \Omega, \qquad \operatorname{div} \boldsymbol{u}_1 = 0 \quad \text{in} \quad \Omega, \qquad \boldsymbol{u}_1 = \boldsymbol{0} \quad \text{on} \quad \Gamma; \tag{4}$$

$$\alpha \boldsymbol{u}_2 - \nu \Delta \boldsymbol{u}_2 + \nabla p_2 = \boldsymbol{0} \quad \text{in} \quad \omega, \qquad \operatorname{div} \boldsymbol{u}_2 = 0 \quad \text{in} \quad \omega, \qquad \boldsymbol{u}_2 = \boldsymbol{g} - \boldsymbol{u}_1 \quad \text{on} \quad \gamma \tag{5}$$

For (5) we use a double layer boundary integral formulation (Section 3) to obtain the velocity potential, $\boldsymbol{\mu}$, on the boundary γ. Solution $\boldsymbol{u}_2$ for an arbitrary point in the interior of ω is the convolution of the double layer kernels with the velocity potential. The solution of the original problem (3) is $\boldsymbol{u} = \boldsymbol{u}_1 + \boldsymbol{u}_2$, $p = p_1 + p_2$.

A discontinuous extension of $\boldsymbol{u}_2$ in Ω, $\boldsymbol{u}_3$, can be chosen so that all the interface jumps can be computed semi-analytically. By tracking the intersection of the interface with the background grid and using the jump relations, we employ Taylor expansions to correct the stencil truncation error [3].

$$\alpha \boldsymbol{u}_3 - \nu \Delta \boldsymbol{u}_3 + \nabla p_3 = 0 \quad \text{in} \quad \Omega, \quad \operatorname{div} \boldsymbol{u}_3 = 0, \quad \text{in} \quad \Omega, \quad \boldsymbol{u}_3 = \boldsymbol{u}_2, \quad \text{on} \quad \Gamma, \tag{6}$$

$$[[\boldsymbol{u}_3]]_\gamma = \boldsymbol{\mu}, \quad [[-p_3 \boldsymbol{n} + \nu(\nabla \boldsymbol{u}_3 + \nabla \boldsymbol{u}_3^T)\boldsymbol{n}]]_\gamma = 0. \tag{7}$$

Numerically, this problem is solved using the same solver used for the problem (4), but with a right-hand side that takes into account the interface jumps computed from the velocity potential.

The EBI method can be summarized as follows:
For each time step,

1. compute $\boldsymbol{b}$ using a semi-Lagrangian method;
2. solve the problem (4) on the simpler domain Ω;
3. solve the boundary integral problem derived from (5) on γ to obtain the velocity potential;
4. compute the right-hand side corrections from the velocity potential;
5. solve the second regular problem on Ω with the computed right-hand side;
6. add the solutions from steps 2 and 5 to obtain the complete solution on ω.

Let us emphasize that steps 2-6 above are carried out exactly as in the Stokes case [3].

3. THE DOUBLE LAYER FORMULATION FOR THE MODIFIED STOKES EQUATIONS

In this section we examine a problem of the form (3) with $\boldsymbol{b} = \boldsymbol{0}$. We also assume that $\omega \subset \mathbb{R}^2$ is bounded and and has C^2-continuous boundary. We use an indirect formulation based on double layer potentials. We limit our discussion to the simply connected interior Dirichlet problem. The extension of EBI to exterior and Neumann problems is very similar to the interior problem. We use the notation

$$\mathcal{C}[w](x) := \int_\gamma \mathcal{C}(\mathbf{x}, \mathbf{y}) \boldsymbol{w}(\mathbf{y})\, d\gamma(\mathbf{y}),$$

to denote the convolution for a kernel $\mathcal{C}$; $\mathcal{C}(\mathbf{x}, \mathbf{y})\boldsymbol{w}$ is a dot product for vector kernels and matrix-vector product for matrix kernels.

We can write the velocities as boundary potentials:

$$\boldsymbol{u}(\mathbf{x}) = \mathcal{D}[\boldsymbol{\mu}](\mathbf{x}), \quad \mathbf{x} \quad \text{in} \quad \omega, \tag{8}$$

$$p(\mathbf{x}) = \mathcal{K}[\boldsymbol{\mu}](\mathbf{x}), \quad \mathbf{x} \quad \text{in} \quad \omega. \tag{9}$$

Here $\boldsymbol{\mu}$ is the hydrodynamic potential.

For the steady Stokes operator the double layer potential is given by

$$\mathcal{D}_0[\boldsymbol{w}](\mathbf{x}) := \frac{1}{\pi}\int_\gamma \frac{\mathbf{r}\otimes\mathbf{r}}{\rho^2}\,\frac{\mathbf{r}\cdot\boldsymbol{n}(\mathbf{y})}{\rho^2}\boldsymbol{w}(\mathbf{y})\,d\gamma(\mathbf{y}); \tag{10}$$

$\mathbf{x}$ is the observation point, $\mathbf{y}$ is the source point, $\mathbf{r} := \mathbf{x}-\mathbf{y}$, $\rho = \|\mathbf{r}\|_2$, $\boldsymbol{n}(\mathbf{y})$ is the outward surface normal at a boundary point $\mathbf{y}$, and $\otimes$ is the tensor product of two vectors.

The corresponding double layer potential for the modified Stokes equations is more complicated. An important parameter is the ratio between the zeroth-order term and the viscous term $\lambda := \sqrt{\frac{\alpha}{\nu}}$. We also use σ to denote $\rho\lambda$.

The double layer potential for the modified Stokes equations is given by the following formula:

$$\mathcal{D}[\boldsymbol{w}](\mathbf{x}) := \mathcal{D}_0[\boldsymbol{w}](\mathbf{x}) + \mathcal{D}_\lambda[\boldsymbol{w}](\mathbf{x}), \tag{11}$$

where $\mathcal{D}_\lambda$ is

$$\begin{aligned}\mathcal{D}_\lambda[\boldsymbol{w}](\mathbf{x}) &= \int_\gamma \mathcal{D}_\lambda(\mathbf{x},\mathbf{y})\,d\gamma(\mathbf{y}) = \\ &= \frac{1}{\pi}\int_\gamma v_1(\sigma)\Big(\frac{\boldsymbol{n}(\mathbf{y})\otimes\mathbf{r}}{\rho^2} + \frac{\mathbf{r}\cdot\boldsymbol{n}(\mathbf{y})}{\rho^2}\mathbf{I}\Big)\boldsymbol{w}(\mathbf{y}) \\ &\qquad + v_2(\sigma)\frac{\mathbf{r}\otimes\mathbf{r}}{\rho^2}\frac{\mathbf{r}\cdot\boldsymbol{n}(\mathbf{y})}{\rho^2}\boldsymbol{w}(\mathbf{y}) + v_3(\sigma)\frac{\mathbf{r}\otimes\boldsymbol{n}(\mathbf{y})}{\rho^2}\boldsymbol{w}(\mathbf{y})\,d\gamma(\mathbf{y}).\end{aligned} \tag{12}$$

The functions v_1, v_2, v_3 are defined using modified Bessel functions of second kind of zero and first order k_0 and k_1 ([1],p.379). We also define an auxiliary function $\beta(\sigma)$ as

$$\beta(\sigma) = \frac{1}{\sigma^2} + \mathrm{k}_0(\sigma) + \frac{2\mathrm{k}_1(\sigma)}{\sigma}. \tag{13}$$

Then

$$v_1(\sigma) = \frac{2\beta(\sigma) + \sigma\mathrm{k}_1(\sigma)}{2}, \tag{14}$$

$$v_2(\sigma) = -4\beta(\sigma) - \sigma\mathrm{k}_1(\sigma) - 1, \tag{15}$$

$$v_3(\sigma) = \frac{2\beta(\sigma)+1}{2}. \tag{16}$$

These formulas are derived in the appendix. The corresponding pressure is computed by taking the divergence of the double layer potential and grouping terms together in $\nabla p = \Delta\boldsymbol{u} - \alpha\boldsymbol{u}$. Let $\mathcal{K}_0$ be the pressure double layer kernel for the steady Stokes equations:

$$\mathcal{K}_0 := -\frac{1}{2\pi}\nabla_x\frac{\mathbf{r}\cdot\boldsymbol{n}}{\rho^2}$$

Let $\mathcal{K}_\lambda$ be the pressure derived from the double layer kernel $\mathcal{D}_\lambda$.

$$\mathcal{K}_\lambda := \frac{1}{2\pi}\lambda^2\log\frac{1}{\rho}$$

Then the double layer potential of the pressure is given by

$$\mathcal{K}[\boldsymbol{\mu};\nu,\lambda] = \frac{1}{\nu}(\mathcal{K}_\lambda[\boldsymbol{\mu}\cdot\boldsymbol{n}] + \mathcal{K}_0[\boldsymbol{\mu}]). \tag{17}$$

The pressure is the sum of a single layer potential of the Laplacian and the gradient of the double layer potential of the Laplacian. The first part comes from the $\alpha \boldsymbol{u}$ term and the second is the same with the Stokes equations. This observation will be useful in deriving the pressure jumps across γ.

In order to use the double layer potentials within EBI method we have to establish the jump properties of $\boldsymbol{u}$ and its corresponding pressure, across the interface. Here we summarize the results for a double layer formulation with Dirichlet boundary conditions. Details are given in the appendix.

- $\mathcal{S}_\lambda$, $\mathcal{D}_\lambda$, and $\nabla_x \mathcal{D}_\lambda$ are continuous across boundary γ; in addition $\mathcal{K}$ is continuous across the interface since it is the single layer of the Laplacian. Thus the double layer for the modified Stokes operator has identical jump properties with the double layer of the steady Stokes operator.
- For smooth geometries the modified Stokes double layer operator is a compact operator.
- The double layer kernel has far field decay, and thus fast multipole methods for elliptic problems are applicable. In particular we can apply the kernel-independent SVD-based fast matrix multiplication [3] *without* modifications.
- The double layer operator has a null space of dimension one for *simply- and multiply-*connected interior domains. It has full rank for exterior problems. However as $\lambda \rightarrow 0$ the contribution of $\mathcal{D}_\lambda$ vanishes and we recover the steady Stokes operator, which has null spaces of higher dimension. If a rank modification based on the interface normal is added, the indirect double layer formulation has a unique solution.

The null space is related to the necessary condition $\boldsymbol{u}$ has to satisfy:

$$\int_\gamma \boldsymbol{u} \cdot \boldsymbol{n} \, d\gamma = 0, \tag{18}$$

which a direct consequence of the conservation of mass. This constraint is an indication that for the interior problem the double layer operator has a null space of dimension at least one. To ensure uniqueness of th solution, we use the following modification of the double layer operator:

$$\mathcal{N}[\boldsymbol{w}](\mathbf{x}) := \int_\gamma \mathcal{N}(\mathbf{x},\mathbf{y}) \boldsymbol{w}(\mathbf{y}) \, d\gamma(\mathbf{y}) = \int_\gamma \boldsymbol{n}(\mathbf{x}) \otimes \boldsymbol{n}(\mathbf{y}) \boldsymbol{w}(\mathbf{y}) \, d\gamma(\mathbf{y}). \tag{19}$$

We solve for $\boldsymbol{u}$ using

$$\boldsymbol{u}(\mathbf{x}) = -\frac{1}{2}\boldsymbol{\mu}(\mathbf{x}) + \mathcal{D}[\boldsymbol{\mu}](\mathbf{x}) + \mathcal{N}[\boldsymbol{\mu}](\mathbf{x}), \quad \mathbf{x} \quad \text{on} \quad \gamma. \tag{20}$$

Taking limits to the boundary from the interior and exterior regions we obtain

$$\boldsymbol{u}(\mathbf{x}) = -\frac{1}{2}\boldsymbol{\mu}(\mathbf{x}) + \mathcal{D}[\boldsymbol{\mu}](\mathbf{x}), \quad \mathbf{x} \quad \text{on} \quad \gamma \tag{21}$$

We discretize (20) by the Nyström method combined with the composite trapezoidal rule which achieves superalgebraic convergence for smooth data. To simplify exposition, we assume ω to be simply connected in the remaining part of this section. Let $[0, 2\pi]$ be

the curve parameter domain and n the number of discretization points with $h = 2\pi/n$. We discretize by:

$$\boldsymbol{u}(\mathbf{x}(ih)) = -\frac{1}{2}\boldsymbol{\mu}(ih) + \frac{1}{h}\sum_{j=1}^{n} \mathcal{D}(\mathbf{x}(ih), \mathbf{y}(jh))\boldsymbol{\mu}(\mathbf{y}(jh)) \, \|\nabla \mathbf{y}(jh)\|_2 \tag{22}$$

$$+ \boldsymbol{n}(\mathbf{x}(ih)) \sum_{j=1}^{n} \boldsymbol{\mu}(\mathbf{y}(jh)) \cdot \boldsymbol{n}(\mathbf{y}(jh) \, \|\nabla \mathbf{y}(jh)\|_2, \quad i = 1, \ldots, n. \tag{23}$$

which results in a dense $2n \times 2n$ linear system. Here $\mathbf{y}(\cdot)$ is the parameterization of γ.

One difficulty with the modified Stokes operator is that the accuracy of the quadrature rule decreases as λ increases. Although $\mathcal{D}_\lambda$ is bounded, it is highly peaked (i.e. its derivatives become nearly unbounded) and thus standard trapezoidal rule will not be as effective. For this reason we use quadrature weights which depend on the evaluation point. Since we want to use fast matrix multiplication methods, the underlying rule is still the trapezoidal rule and quadrature weight modification is used only for a small number of points. For details see [21] and [9].

Jump computation. Equation (8) is defined for points inside ω. We can use exactly the same relation to extend $\boldsymbol{u}$ in $\mathbb{R}^2/\bar{\omega}$.

The resulting field is discontinuous across the interface. From the properties of the double layer kernel for an interior problem we have the following jump relations:

$$\begin{aligned} \boldsymbol{u}_e - \boldsymbol{u}_i &= \boldsymbol{\mu}, \\ \boldsymbol{\sigma}_e - \boldsymbol{\sigma}_i &= 0, \\ (\nabla \boldsymbol{u}_e - \nabla \boldsymbol{u}_i)\boldsymbol{t} &= \dot{\boldsymbol{\mu}}. \end{aligned} \tag{24}$$

In each formula, the left-hand side is the difference of the limits from the exterior and interior of the domain. The last equation can be obtained by differentiating the first equation in the tangential direction;$\dot{\boldsymbol{\mu}}$ is the derivative of the potential with respect the parameterization of the curve: $\dot{\boldsymbol{\mu}} = d\boldsymbol{\mu}(\mathbf{y}(t))/dt$. Similar relations can be derived for the pressure. Higher-order derivatives can be obtained by differentiating (24) augmented with the continuity of the momentum equation across the interface.

4. SEMI-LAGRANGIAN APPROXIMATION

In order to obtain an efficient and accurate time stepping scheme we use a semi-Lagrangian formulation [5]. The relation between the the Lagrangian and Eulerian description of the acceleration term is given by

$$\frac{d\boldsymbol{u}(\mathbf{x}(t), t)}{dt} = \frac{\partial \boldsymbol{u}(\mathbf{x}, t)}{\partial t} + (\nabla \boldsymbol{u}(\mathbf{x}, t))\boldsymbol{u}(\mathbf{x}, t). \tag{25}$$

were $\mathbf{x}(t) := \mathbf{x}(\boldsymbol{p}, t)$ is the fluid particle occupyingposition $\mathbf{x}$ at time t; $\boldsymbol{p}$ is its position in the reference configuration [8]. Instead of discretizing the right-hand side, we discretize the left-hand side; this approach requires particle tracking for $\mathbf{x}(t)$.

For notational convenience let

$$\bar{\boldsymbol{u}}_0 = \boldsymbol{u}(\mathbf{x}(t - \delta t), t - \delta t), \text{ and } \bar{\boldsymbol{u}}_{00} = \boldsymbol{u}(\mathbf{x}(t - 2\delta t), t - 2\delta t).$$

To compute the velocity at the previous time step, we have to compute $\mathbf{x}(t - \delta t)$; i.e. we have to locate the starting point of the flow particle that arrived to the grid point $\mathbf{x}$ (Figure 4).

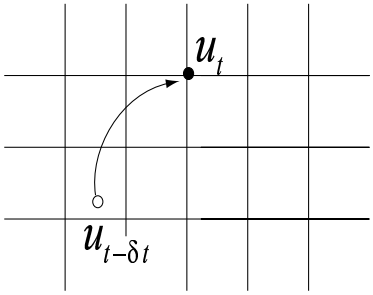

FIG. 1 Semi-Lagrangian formulation. To discretize in time we have to locate the point from which a particle with velocity $\boldsymbol{u}(t-\delta t)$ traveled to the grid point with velocity $\boldsymbol{u}(t)$.

In our numerical experiments we have used a first order backward Euler scheme, and a two-step second order scheme:

$$\frac{d\boldsymbol{u}}{dt} = \tfrac{1}{\delta t}(\boldsymbol{u}-\bar{\boldsymbol{u}}_0) = -(-\nu\Delta(\boldsymbol{u})+\nabla p), \tag{26}$$

$$\frac{d\boldsymbol{u}}{dt} = \tfrac{1}{\delta t}(\tfrac{3}{2}\boldsymbol{u}-2\bar{\boldsymbol{u}}_0+\tfrac{1}{2}\bar{\boldsymbol{u}}_{00}) = -(-\nu\Delta(\boldsymbol{u})+\nabla p). \tag{27}$$

To compute $\bar{\boldsymbol{u}}_0$ and $\bar{\boldsymbol{u}}_{00}$ we solve

$$\frac{d\mathbf{x}(t)}{dt} = \boldsymbol{u}(\mathbf{x}(t),t), \tag{28}$$

using first and second order schemes accordingly. If $\delta\mathbf{x}$ is $\mathbf{x}(t)-\mathbf{x}(t-\delta t)$, the we obtain the following first-order accurate nonlinear equation (for $\delta\mathbf{x}$)

$$\delta\mathbf{x} = \delta t\boldsymbol{u}(\mathbf{x}(t)-\delta\mathbf{x}, t-\delta t), \tag{29}$$

which we solve iteratively by taking a few fixed point steps ($\delta\mathbf{x}_{k+1} = \delta t\boldsymbol{u}(\mathbf{x}(t)-\delta\mathbf{x}_k, t-\delta t)$). The interpolation of $\boldsymbol{u}$ has to be done carefully to avoid excessive dissipation. We use B-splines which can be shown that have very good dissipation and dispersion properties [20]. For the second order scheme we use a similar approach with the midpoint rule, $\delta\mathbf{x} = \delta t\ \boldsymbol{u}(\mathbf{x}(t)-\delta/2\ \mathbf{x}, t-\delta t/2)$. The velocity at time $t-\delta t/2$ is evaluated by extrapolation: $\boldsymbol{u}(t-\delta t/2) = 3/2\ \boldsymbol{u}(t-\delta t) - 1/2\ \boldsymbol{u}(t-2\delta t)$.

5. NUMERICAL EXPERIMENTS

In this section we present numerical results that illustrate the effectiveness of the EBI method and its individual components. We test the semi-Lagrangian solver, the modified Stokes boundary integral solver, the effectiveness of the SVD-based acceleration and the overall method.

Regular Grid Solver. We have chosen to solve for the velocity and pressure simultaneously using a finite element method with $Q1$-$Q1$ bilinear elements with stabilization [16]. In [3] we show that optimal convergence rates are obtained (second order for velocities, first order for pressures) provided we include second-order accurate jump information. We also provide details on the numerical methods required to solve the systems (we use a

two level domain decomposition preconditioner which is optimal for the Stokes problem, [11]).

First we test the semi-Lagrangian approach using an exact solution, the Taylor vortex flow, and then using the standard test of the lid-driven cavity problem. In this tests we only examine the regular grid solver, therefore no integral equations are used. The Taylor vortex solution is given by:

$$\boldsymbol{u} = e^{-2t\nu} \begin{cases} -\cos x \sin y \\ -\sin x \cos y, \end{cases} \quad p = -\frac{1}{4} e^{-4t\nu} (\cos 2x + \cos 2y). \tag{30}$$

An example of a vortex flow is depicted in Figure 2. The solution was obtain using the FEM-based semi-Lagrangian method on a 64^2 grid for Re=100.

FIG. 2 Streamlines for the Taylor vortex flow, which is an exact solution to the unsteady Navier-Stokes equations.

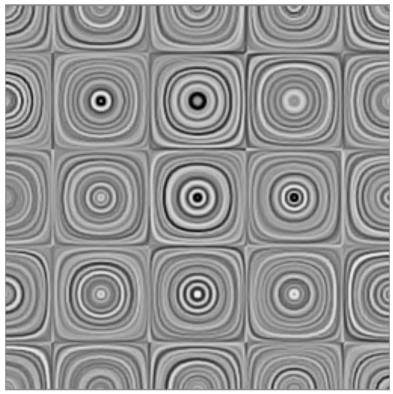

In the following table we give convergence rates for the Taylor vortex flow as a function of the CFL number for different grids. We compare semi-Lagrangian and Eulerian methods. In the latter case the convective term is discretized explicitly by

$$(\nabla \boldsymbol{u})\boldsymbol{u} \approx 3/2\ (\nabla \boldsymbol{u}_0)\boldsymbol{u}_0 - 1/2\ (\nabla \boldsymbol{u}_{00})\boldsymbol{u}_{00}.$$

The results are summarized in Table 1. We compare different grid sizes, different time steps and different Reynolds numbers.

In Figure 3 we show results for a computation of a lid-driven cavity problem for Reynolds number 10,000. In this regime the flow is unsteady and we show different snapshots of the flow.

Boundary integral solver In Table 2 we present results that illustrate the efficiency of the SVD acceleration on the modified Stokes equations. We compute the flow around 36 identical uniformly spaced circles. In this case the exact solution is a modified Stokeslet. In all cases we obtain machine accuracy for the velocity and increasing accuracy for the pressure. Note that as $\lambda \to 0$ the kernel approaches the standard Stokes operator and thus for multiply connected geometries it will be rank defficient. As a consequence for smaller λ values the modified Stokes problem becomes more ill-conditioned. This was not a problem for $\lambda = 100$. The ill-conditioning also explains why the solution time is in general smaller for $\lambda = 100$.

FIG. 3 Time snapshot of a lid-driven cavity flow for $Re = 10,000$ on a 280^2 grid with a CFL=15. The first row shows snapshots on the onset of the flow and the bottom show snapshot from the end of the simulation. The flow for this Reynolds number is known to be unsteady. the for the 280^2 grid.

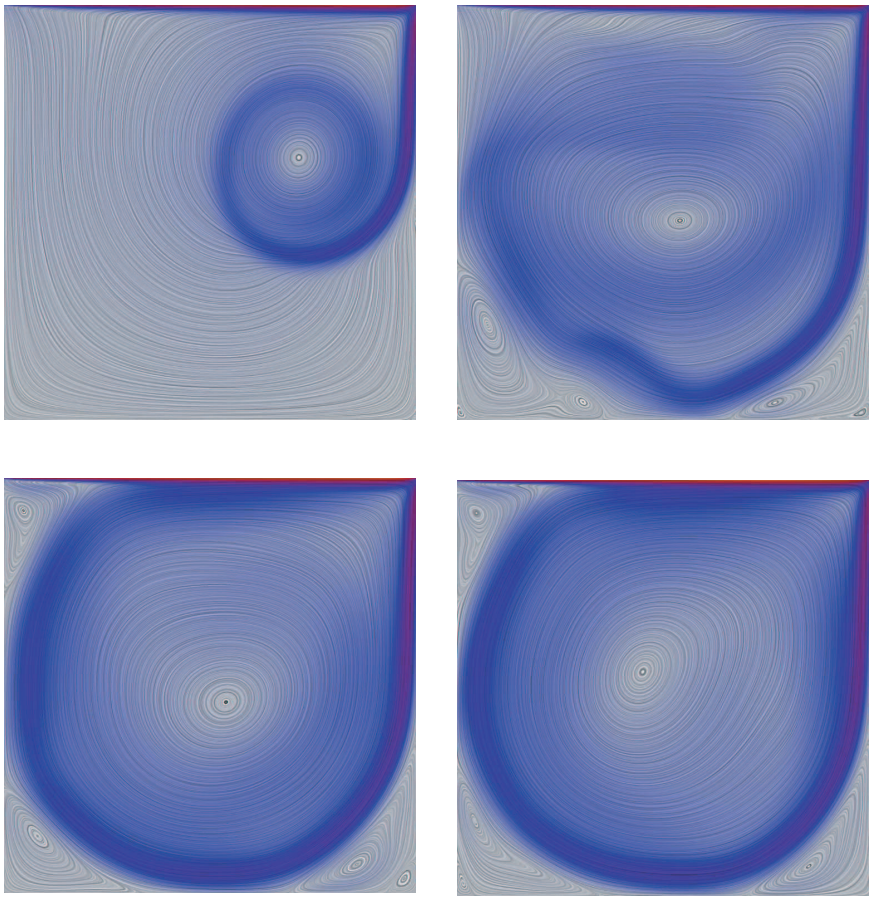

TABLE 1
$L_\infty(\omega, t)$ normalized by the L_∞ norm of the exact solution) for the velocity as a function of δt and the Reynolds number. *Euler* shows error for the Eulerian reference. In parentheses we give the time step as a function of the spatial grid size. In the next columns, *sl 4,8,16* we give results for the semi-Lagrangian method with time steps which are 3, 8, and 16 times larger than that of Eulerian method. The time horizon is 4π, which corresponds to two flow revolutions.

	Re = 10^2			
grid size	*Euler*($2h$)	*sl 4*	*sl 8*	*sl 16*
64^2	1.02×10^{-3}	4.19×10^{-3}	6.83×10^{-3}	1.15×10^{-2}
128^2	2.44×10^{-4}	1.10×10^{-3}	1.55×10^{-3}	3.93×10^{-3}
256^2	6.80×10^{-5}	3.62×10^{-4}	4.59×10^{-4}	9.39×10^{-3}
	Re = 10^4			
grid size	*Euler*($h/2$)	*sl 4*	*sl 8*	*sl 16*
64^2	4.56×10^{-2}	1.16×10^{-1}	1.98×10^{-1}	2.21×10^{-1}
128^2	1.57×10^{-2}	3.50×10^{-2}	5.18×10^{-2}	5.32×10^{-2}
256^2	4.44×10^{-3}	9.17×10^{-3}	1.73×10^{-2}	1.79×10^{-2}

TABLE 2
Comparison between the dense matrix matrix-vector multiplication and the SVD-based matrix-vector multiplication for two different λ values for a geometry with 36 circles; the exact solution is the modified Stokeslet. Setup time includes the construction of the matrix; no preconditioning is used. Solve time is the time used by GMRES solver. We see that as the problem scales, the dense computation grows quadratically, while SVD computation scales almost linearly.

domain, solution	N	matrix	setup	solve	$\|\mathbf{u}\|_{err}$	p_{err}
$\lambda = 1$	768	dense	3.38	10.6	2.34×10^{-08}	2.67×10^{-07}
		svd	4.08	5.18	2.44×10^{-08}	2.65×10^{-06}
Stokeslet	1536	dense	13.5	41.1	2.31×10^{-09}	2.73×10^{-08}
		svd	7.81	12.2	2.27×10^{-08}	2.66×10^{-06}
	3072	dense	68.2	165	2.13×10^{-10}	2.47×10^{-08}
		svd	16.7	26.5	2.00×10^{-09}	1.99×10^{-07}
	6144	dense	318	763	2.22×10^{-11}	2.68×10^{-09}
		svd	16.6	55.8	2.00×10^{-09}	1.99×10^{-07}
$\lambda = 100$	768	dense	3.45	2.30	1.16×10^{-05}	2.73×10^{-02}
		svd	3.38	1.10	1.15×10^{-05}	2.73×10^{-02}
Stokeslet	1536	dense	15.0	9.00	1.45×10^{-06}	3.42×10^{-03}
		svd	7.51	2.32	1.47×10^{-06}	3.50×10^{-03}
	3972	dense	56.1	35.5	1.73×10^{-07}	4.10×10^{-04}
		svd	15.8	4.98	1.82×10^{-07}	4.31×10^{-04}
	6144	dense	336	142	1.99×10^{-08}	4.01×10^{-05}
		svd	32.9	10.6	2.08×10^{-08}	4.88×10^{-05}

Embedded boundary integral solver. We present preliminary results for the unsteady Stokes and Navier-Stokes problems. We have chosen an synthetic solution for the steady Stokes given by

$$\boldsymbol{u} = 2\left\{-x^2y, y^2x\right\}, \; p = \sin(xy), \; \boldsymbol{b} = 4\nu\left\{y(1+\cos(xy), -x(1+\cos(xy)\right\}.$$

We use the unsteady solver to "march" to the steady state solution. The initial guess an the initial conditions are zero; the boundary conditions are mollified to their exact values on time period which is 10% of the total time horizon. In Figures 4 and 5 we show the exact solution and the error distribution for a 128^2 and a 256^2 grid respectively.

FIG. 4 Solution and error for the for the 128^2 grid.

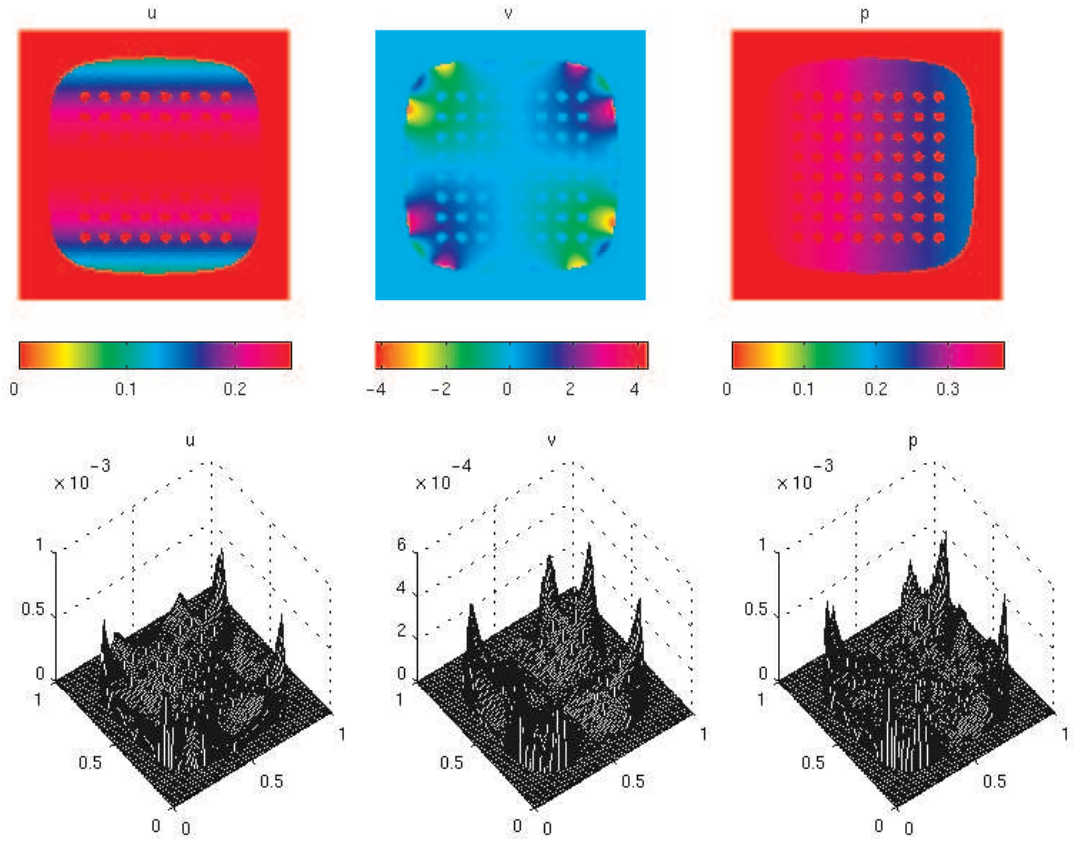

Pointwise error norms for the first-order and second-order accurate jump corrections are given in Table 3. The first and second columns give the maximum pointwise absolute errors for the velocity and pressure; and the third and fourth columns give results for second order accurate jumps. We can observe suboptimal rates for the first-order jumps and optimal convergence rates for the second order jumps. For this type of flow the influence of the time stepping accuracy is negligible.

We also present results for the Taylor vortex flow. We solve this problem for two different geometries by restricting the solution to the given geometry. We vary the Reynolds

FIG. 5 Solution and error for the for the 256^2 grid.

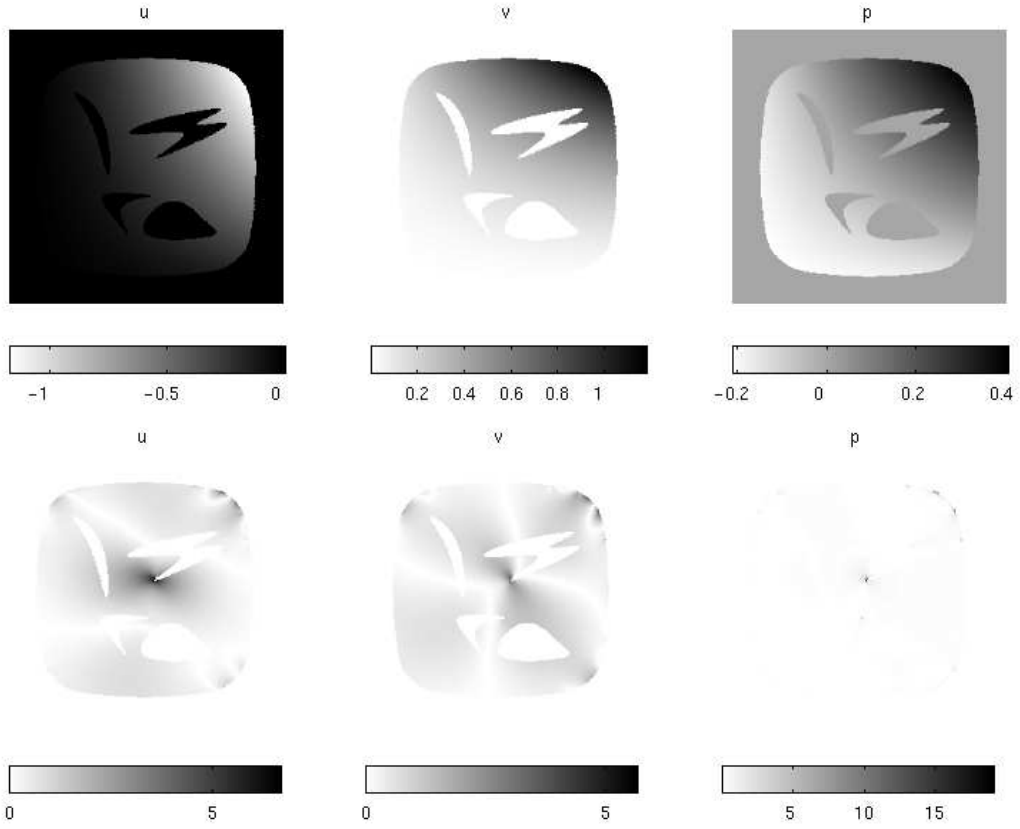

TABLE 3
Pointwise absolute error for the velocity and pressure.

	first-order		*second-order*	
grid size	u_{err}	p_{err}	u_{err}	p_{err}
32^2	1.38×10^{-1}	9.82×10^{-1}	4.19×10^{-3}	1.56×10^{-1}
64^2	4.98×10^{-2}	7.86×10^{-1}	1.51×10^{-3}	7.91×10^{-2}
128^2	1.49×10^{-2}	4.38×10^{-1}	4.68×10^{-4}	4.78×10^{-2}
256^2	5.65×10^{-3}	3.57×10^{-1}	1.18×10^{-4}	2.33×10^{-2}

number and the time stepping in order to assess the accuracy of the boundary integral solver.

In Table 4 we present the results for essentially the same problem as for Table 1 only this time the flow is restricted to a circle inside the regular domain. Comparing the regular grid solution with the EBI solution we observe that the accuracy of the Eulerian method

FIG. 6 A time snapshot for the Taylor vortex flow confined to a circle. First row: the exact solution; second row: the pointwise error; third row: the vorticity.

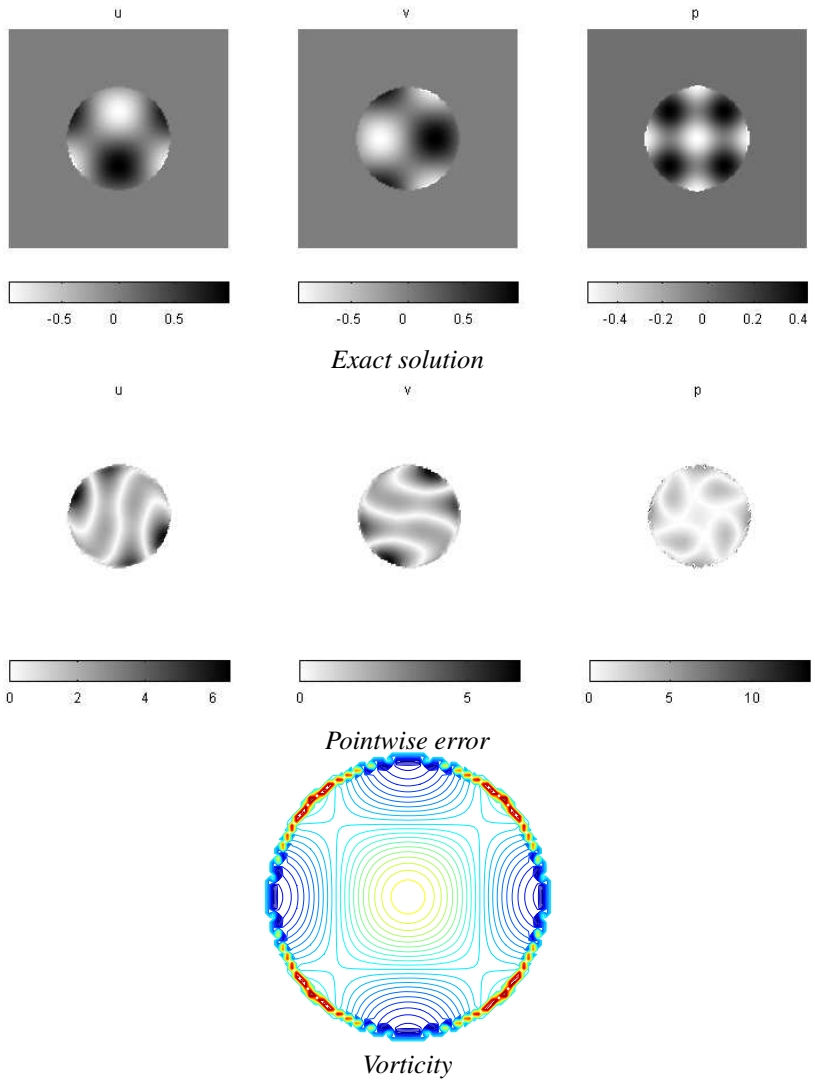

deteriorates, but the accuracy of the semi-Lagrangian methods improves. The reason for the former is that we only include zeroth order corrections for the convective term across the interface: we take into account the jump in the velocity and not the jump in its derivative. The semi-Lagrangian approach performs well, and we maintain optimal convergence rates.

In the next example we solve for a flow past a circle which is inside a channel (channel flow with obstacle). We only give qualitative results since our problem setup does not correspond very well to the physics:(1) since we only use C^2-continuous boundaries, we use a Lamé curve ($(x/a)^n + (y/b)^n = R^n$), instead of a rectangle; (2) the outflow conditions are Dirichlet instead of the more appropriate Neumann conditions;(3) the downwind length is

TABLE 4
Normalized $L_\infty(\omega, t)$ error for the velocity as a function of δt and the Reynolds number. *Euler* shows error for the Eulerian reference. In parentheses we give the time step as a function of the spatial grid size. In the next columns, *sl 4,8,16* we give results for the semi-Lagrangian method with time steps which are 3, 8, and 16 times larger than that of Eulerian method. The time horizon is 4π, which corresponds to two flow revolutions.

	Re = 10^2			
grid size	*Euler*($2h$)	*sl 4*	*sl 8*	*sl 16*
64^2	2.83×10^{-3}	2.77×10^{-3}	3.41×10^{-3}	9.95×10^{-3}
128^2	6.97×10^{-4}	7.45×10^{-3}	9.13×10^{-3}	3.35×10^{-3}
256^2	2.49×10^{-4}	1.79×10^{-4}	2.65×10^{-4}	8.76×10^{-4}

relatively short, thus the flow is artificially changed to satisfy the Dirichlet boundary conditions. The computational domain we use is only $4d \times 8d$, where d is the diameter of the cylinder. The boundary conditions in inlet and outlet are those of an unobsructed channel flow (Poiseuille). Figure 7 shows streamlines for the Reynolds number equal to 100. For an exterior problem such flow is unsteady but still laminar. However for the chosen problem setup the resulting flow is steady.

FIG. 7 Flow around a cylinder for Reynolds number 100.

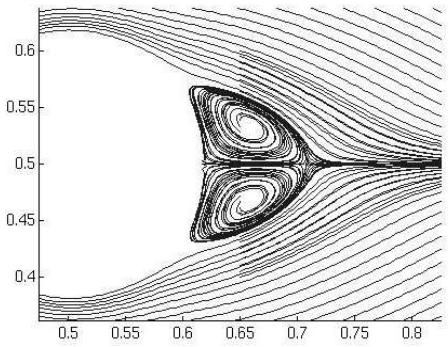

In the final example we solve a flow around an irregular geometry using a uniform flow profile for the inlet and outlet. The Reynolds number is based on the dimensions of the enclosing box (length=1). In figures 8 and 9 we show snapshots of the velocity, pressure and vorticity fields from the initiation of the flow until it reaches a steady state.

6. CONCLUSIONS AND EXTENSIONS

We have presented a second-order accurate solver for the unsteady Navier-Stokes equations on arbitrary domains. We use a hybrid boundary integral, regular grid finite element formulation to bypass the need for domain mesh generation on arbitrary geometries. We

FIG. 8 Snapshots for Re=150, CFL=8, on 256^2 grid

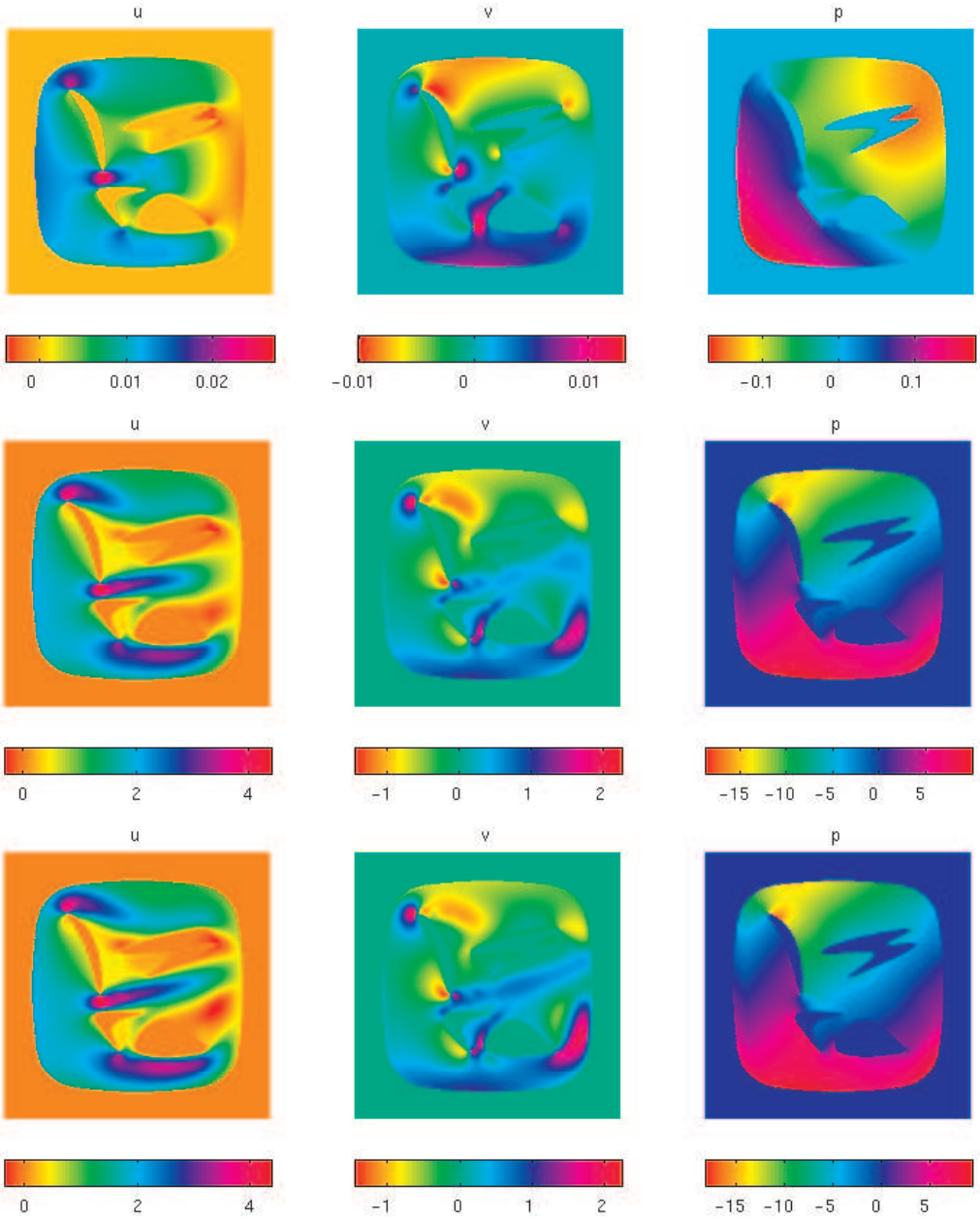

FIG. 9 Snapshots of vorticity for Re=150, CFL=8, on 256^2 grid

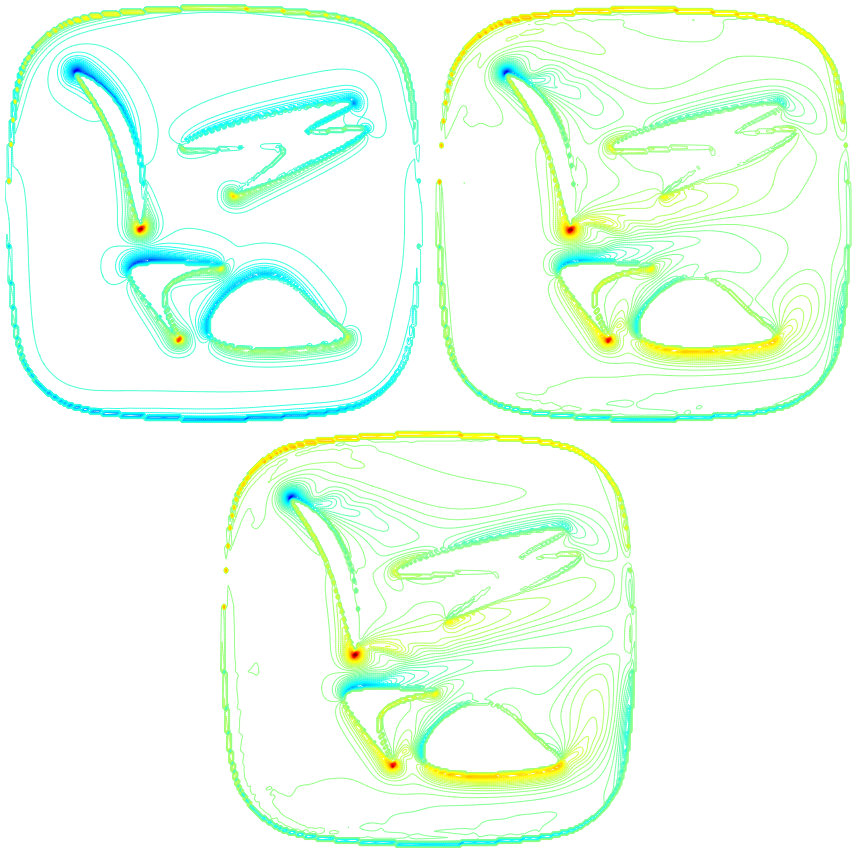

employ an efficient double layer formulation for the resulting integral equations. At each time step the method requires two regular grid solves and one integral equation solve.

One restriction of the method, as we have presented it, is the stringent requirements on the regularity of the boundary geometry. This can be circumvented by replacing the jump computation for the stencils corrections by direct evaluation at the stencil points: the jump terms can be computed to machine accuracy by plugging the exact solution in the stencils that cross the boundary. The exact solution can be obtain by direct evaluation of the velocity using the integral representation. This requires adaptive quadratures—but only for the points close to a corner.

APPENDIX A: BOUNDARY INTEGRAL FORMULATION FOR THE UNSTEADY STOKES EQUATIONS

A.1. Double layer potential for the modified Stokes equations

To construct the modified Stokeslet we compute $\boldsymbol{u}^*(\mathbf{x}) := \boldsymbol{u}^*(\mathbf{x};\mathbf{y},\mathbf{e})$, and $p^*(\mathbf{x}) := p^*(\mathbf{x};\mathbf{y},\mathbf{e})$, the solution of a free-space problem with a point load located at $\mathbf{y}$ with direction $\mathbf{e}$:

$$\begin{aligned} \alpha\boldsymbol{u}^*(\mathbf{x}) - \nu\Delta\boldsymbol{u}^*(\mathbf{x}) + \nabla p^*(\mathbf{x}) &= \delta(\mathbf{x}-\mathbf{y})\mathbf{e}, && (31)\\ \operatorname{div}\boldsymbol{u}^*(\mathbf{x}) &= \mathbf{0} && (32)\\ \boldsymbol{u}(\mathbf{x}) \to \mathbf{0} \quad &\text{as} \quad \mathbf{x}\to\infty \end{aligned}$$

After taking divergence of equation (31) and using equation (32), we obtain

$$\Delta p^* = \operatorname{div}(\delta\mathbf{e}) = \operatorname{div}(-\Delta\phi^*\mathbf{e}) = \Delta(-\nabla\phi^*\cdot\mathbf{e})$$

where $\phi^* = \frac{1}{2\pi}\ln 1/\rho$ is the fundamental solution of Laplace operator with $\boldsymbol{r} = \mathbf{x}-\mathbf{y}$ and $\rho = \|\boldsymbol{r}\|_2$. Therefore $p^* = -\nabla\phi^*\cdot\mathbf{e}$. Substituting p^* into (31) we get

$$\begin{aligned} (\alpha-\nu\Delta)\boldsymbol{u}^* + \nabla(-\nabla\phi^*\cdot\mathbf{e}) &= -\Delta\phi^*\mathbf{e} \qquad (-\Delta\phi^* = \delta)\\ (\alpha-\nu\Delta)\boldsymbol{u}^* &= -\Delta\phi^*\mathbf{e} + \nabla(\nabla\phi^*\cdot\mathbf{e})\\ &= (-\Delta\mathsf{I} + \nabla\otimes\nabla)\phi^*\mathbf{e}\\ \boldsymbol{u}^* &= \frac{1}{\nu}(\frac{\alpha}{\nu}-\Delta)^{-1}((-\Delta\mathsf{I}+\nabla\otimes\nabla)\phi^*\mathbf{e})\\ &= \frac{1}{\nu}(-\Delta\mathsf{I}+\nabla\otimes\nabla)(\frac{\alpha}{\nu}-\Delta)^{-1}\phi^*\mathbf{e} \end{aligned}$$

Let ψ^* satisfy

$$\begin{aligned} (\lambda^2-\Delta)\psi^* &= \phi^* \text{ or equivalently}\\ (\lambda^2\Delta-\Delta^2)\psi^* &= -\delta, \end{aligned}$$

that is, ψ is the fudnamental solution of the modified biharmonic equation. Then it is given by the expression

$$\psi^*(\mathbf{x};\mathbf{y}) = -\frac{1}{2\pi\lambda^2}\rho^2(\ln\rho + \mathrm{k}_0(\lambda\rho)), \tag{33}$$

where k_0 is the modified Bessel function of order zero. Therefore the fundamental solution is obtained by

$$\boldsymbol{u}^*(\mathbf{x};\mathbf{y},\mathbf{e}) = \frac{1}{\nu}(-\Delta\mathsf{I}+\nabla\otimes\nabla)\psi(\mathbf{x};\mathbf{y})\mathbf{e},$$

and by taking $\mathbf{e}$ for each coordinate we can construct the the modified Stokeslet tensor

$$\mathcal{U}(\rho) = \frac{-1}{2\pi\nu\lambda^2}\left\{(-\frac{1}{\sigma^2} - \frac{\mathrm{k}_1(\sigma)}{\sigma} + -\mathrm{k}_0(\sigma))\mathbf{I} + (-\frac{2}{\sigma^2} + b + \frac{2\mathrm{k}_1(\sigma)}{\sigma} + \mathrm{k}_0(\sigma))\frac{\mathbf{r}\otimes\mathbf{r}}{\rho^2}\right\} \tag{34}$$

Combining this equation with the relation for the pressure we can compute the stress tensor of the fundamental solution. Its adjoint, applied to the surface normal, is the double layer potential. The derivation is somewhat lengthy but straightforward.

A.2. Null spaces of the double layer potential operators

Since double layer operator $\mathcal{D}$ is a compact operator, in this section we use the Fredholm alternative ([12],pp. 47–48) to derive the properties of the double layer operator in three cases: bounded domain, unbounded domain and multiply connected domain. Our analysis is based on the analysis for the steady Stokes operator in [10].

The modified stokes equation in ω with boundary γ is

$$\alpha\boldsymbol{u} - \nu\Delta\boldsymbol{u} + \nabla p = \mathbf{0} \quad \text{in} \quad \omega, \quad \operatorname{div}\boldsymbol{u} = 0 \quad \text{in} \quad \omega, \tag{35}$$

LEMMA 1 (Lorentz Identity). *Suppose* $(\boldsymbol{u}, p, \boldsymbol{T})$ *and* $(\boldsymbol{v}, q, \boldsymbol{S})$ *are two solutions of the modified stokes equation, then div* $(\boldsymbol{S}\boldsymbol{u} - \boldsymbol{T}\boldsymbol{v}) = 0$.

LEMMA 2 (Energy Identity). $\int_\omega \alpha\boldsymbol{u}\cdot\boldsymbol{u} + \boldsymbol{T}\cdot\frac{\nabla\boldsymbol{u}+\nabla\boldsymbol{u}^\mathsf{T}}{2} = \int_\gamma(\boldsymbol{T}\boldsymbol{n})\cdot\boldsymbol{u}$

Notice $-q\mathsf{I}\cdot(\nabla\boldsymbol{u}+\nabla\boldsymbol{u}^\mathsf{T}) = -q\operatorname{div}\boldsymbol{u} = 0$, we have $\boldsymbol{T}\cdot\frac{\nabla\boldsymbol{u}+\nabla\boldsymbol{u}^\mathsf{T}}{2} = \frac{1}{2}\nu(\nabla\boldsymbol{u}+\nabla\boldsymbol{u}^\mathsf{T})^2$. Therefore, we can have the following identity:

$$\int_\omega \alpha\boldsymbol{u}^2 + \frac{1}{2}\nu(\nabla\boldsymbol{u}+\nabla\boldsymbol{u}^\mathsf{T})^2 = \int_\gamma(\boldsymbol{T}\boldsymbol{n})\cdot\boldsymbol{u}.$$

LEMMA 3 (Uniqueness). *Boundary value problem equation (35) has unique solution, both for* Ω *bounded or unbounded.*

In the rest of this section, we use subscripts e and i refer to the limits from the interior and exterior of an interface, $\boldsymbol{u}_e$ and $\boldsymbol{u}_i$ denote velocities, while $\boldsymbol{\tau}_e$ and $\boldsymbol{\tau}_i$ denote tractions. From the results of stokes equation, we know that

1. with ϕ as single layer density on boundary γ,

$$\boldsymbol{u}_i - \boldsymbol{u}_e = 0 \quad \boldsymbol{\tau}_i = (\frac{1}{2} - \mathcal{D}^\mathsf{T})\phi \quad \boldsymbol{\tau}_e = (-\frac{1}{2} - \mathcal{D}^\mathsf{T})\phi$$

2. with $\boldsymbol{\mu}$ as double layer density on boundary γ,

$$\boldsymbol{u}_i = (\frac{1}{2} + \mathcal{D})\boldsymbol{\mu} \quad \boldsymbol{u}_e = (\frac{1}{2} + \mathcal{D})\boldsymbol{\mu} \quad \boldsymbol{\tau}_i - \boldsymbol{\tau}_e = 0$$

The following three propositions are about the null space of the double layer potential operators $\mathcal{D}$. We use $N(\cdot)$ to denote the null space of an operator and $R(\cdot)$ to denote the range.

PROPOSITION 1 (Bounded domain). $\dim N(-\frac{1}{2}+\mathcal{D}) = 1$. *For any* $\boldsymbol{\xi}\in N(-\frac{1}{2}+\mathcal{D})$, *the dot product* $(\boldsymbol{\xi}, \boldsymbol{n})$ *does not vanish.*

Proof. First, we prove that $\dim N(-\frac{1}{2}+\mathcal{D}) \geq 1$. Choose any double layer density $\boldsymbol{\mu}$, then $\boldsymbol{u} = (-\frac{1}{2}+\mathcal{D})\boldsymbol{\mu}$ is a solution of modified stokes equation, therefore for $(\boldsymbol{n}, (-\frac{1}{2}+\mathcal{D})\boldsymbol{\mu}) = 0$ by divergence theorem. Then $(-\frac{1}{2}+\mathcal{D}^{\mathsf{T}})\boldsymbol{n} = 0$ which says $\dim N(-\frac{1}{2}+\mathcal{D}^{\mathsf{T}}) \geq 1$. From that, we conclude $\dim N(-\frac{1}{2}+\mathcal{D}) \geq 1$ by the Fredholm alternative.

Next, we prove $\dim N(-\frac{1}{2}+\mathcal{D}) \leq 1$. Suppose there is a $\boldsymbol{\mu}$ with $(-\frac{1}{2}+\mathcal{D}^{\mathsf{T}})\boldsymbol{\mu} = 0$. Viewing $\boldsymbol{\mu}$ as a single layer density, the traction $\boldsymbol{\tau}_e$ vanishes. Hence $(\boldsymbol{u}_e, \boldsymbol{\tau}_e) = 0$. By energy identity, we know $\boldsymbol{u}_i$ can only be zero due to the decay of the solution at infinity. From $\boldsymbol{u}_e = \boldsymbol{u}_i$ for single layer density, we know that $\boldsymbol{u}_i = 0$ This in turns gives interior pressure limit p_i is a constant c. Therefore $\boldsymbol{\tau}_i = c\boldsymbol{n}$ and $\boldsymbol{\mu} = \boldsymbol{\tau}_i - \boldsymbol{\tau}_e = c\boldsymbol{n}$. This is just $\dim N(-\frac{1}{2}+\mathcal{D}^{\mathsf{T}}) \leq 1$. Therefore, $\dim N(-\frac{1}{2}+\mathcal{D}) \leq 1$ by the Fredholm alternative

Finally we prove that $(\boldsymbol{\xi}, \boldsymbol{n}) \neq 0$. Suppose $\boldsymbol{n} \in R(-\frac{1}{2}+\mathcal{D}^{\mathsf{T}})$. Then there is a density $\boldsymbol{\mu}$ such that $(\frac{1}{2}-\mathcal{D}^{\mathsf{T}})\boldsymbol{\mu} = \boldsymbol{n}$ With $\boldsymbol{\mu}$ as single layer density, the corresponding traction $\boldsymbol{\tau}_e$ is just $\boldsymbol{n}$. Therefore $(\boldsymbol{u}_e, \boldsymbol{\tau}_e) = 0$. Due to the energy identity again, it follows that $\boldsymbol{u}_e = 0$ and $\boldsymbol{\tau}_e = 0$; therefore, $(\frac{1}{2}-\mathcal{D}^{\mathsf{T}})\boldsymbol{\mu} = 0$, which is a contradiction. Therefore, $\boldsymbol{n}$ cannot be in the range $R(-\frac{1}{2}+\mathcal{D}^{\mathsf{T}})$ and has a component in $N(-\frac{1}{2}+\mathcal{D})$ since $R(-\frac{1}{2}+\mathcal{D}^{\mathsf{T}})^{\perp} = N(-\frac{1}{2}+\mathcal{D})$. ∎

PROPOSITION 2 (Unbounded domain). $\dim N(-\frac{1}{2}+\mathcal{D}) = 0$

Proof. Suppose $(-\frac{1}{2}+\mathcal{D}^{\mathsf{T}})\boldsymbol{\mu} = 0$. With $\boldsymbol{\mu}$ as a single layer density, the traction $\boldsymbol{\tau}_e$ is zero. Now $(\boldsymbol{u}_e, \boldsymbol{\tau}_e) = 0$. Since the domain now is unbounded, the only solution possible is $\boldsymbol{u}_e = 0$.Since $\boldsymbol{\mu}$ is a single layer, then $\boldsymbol{u}_i = 0$ as well. This gives $\boldsymbol{\tau}_i = 0$ because the fluid domain is now unbounded and $\boldsymbol{\tau}_i$ needs to approach 0 at infinity. It follows that $\boldsymbol{\mu} = \boldsymbol{\tau}_i - \boldsymbol{\tau}_e = 0$ and $\dim N(-\frac{1}{2}+\mathcal{D}^{\mathsf{T}}) = 0$ and $\dim N(-\frac{1}{2}+\mathcal{D}) = 0$. ∎

PROPOSITION 3 (Multiply connected domain). *Suppose the boundary γ consists of a set of curves $\{\gamma_0, \gamma_1, \cdots, \gamma_M\}$, where γ_0 is the outer boundary, then* $\dim N(-\frac{1}{2}+\mathcal{D}) = 1$.

Proof. First, we prove that $\dim N(-\frac{1}{2}+\mathcal{D}) \geq 1$. From proposition 1, we know that there exists a double layer which gives zero velocity in the region bounded by γ_0. We define $\boldsymbol{\xi}_0$ to be the same as this solution on γ_0 and to be zero on $\gamma_i, 1 \leq i \leq M$. Clearly $\boldsymbol{\xi}_0$ is in the null space of $\frac{1}{2}+\mathcal{D}$. Therefore $\dim N(-\frac{1}{2}+\mathcal{D}) \geq 1$.

Next, we prove that $\dim N(-\frac{1}{2}+\mathcal{D}) \leq 1$. The proof proceeds exactly in the same way as for the bounded domain: Suppose $(-\frac{1}{2}+\mathcal{D}^{\mathsf{T}})\boldsymbol{\mu} = 0$. Then with $\boldsymbol{\mu}$ as single layer density, the traction $\boldsymbol{\tau}_e$ vanishes, and $\boldsymbol{u}_i = \boldsymbol{u}_e = 0$ on $\gamma_0, \cdots, \gamma_M$. Then the interior limit of pressure p_i is again an constant c. Therefore $\boldsymbol{\tau}_i = c\boldsymbol{n}$ and $\boldsymbol{\mu} = \boldsymbol{\tau}_e - \boldsymbol{\tau}_i = -c\boldsymbol{n}$, this means $\dim N(-\frac{1}{2}+\mathcal{D}^{\mathsf{T}}) \leq 1$. Using Fredholm alternative, we have again $\dim N(-\frac{1}{2}+\mathcal{D}) \leq 1$. ∎

Remark 1. Suppose $\boldsymbol{n}_0$ is the function which has the same value as $\boldsymbol{n}$ on γ_0 and vanishes on $\gamma_i, 1 \leq i \leq M$. Suppose $(\frac{1}{2}-\mathcal{D}^{\mathsf{T}})\boldsymbol{\mu} = \boldsymbol{n}_0$ then $\boldsymbol{\tau}_e = \boldsymbol{n}_0$. Since $\boldsymbol{u}_e$ is single layer, $(\boldsymbol{u}_e, \boldsymbol{n}_0) = 0$. Therefore $(\boldsymbol{u}_e, \boldsymbol{\tau}_e)_{\gamma_0} = 0$ and both $\boldsymbol{u}_e$ and $\boldsymbol{\tau}_e$ vanish on γ_0. Then $(\frac{1}{2}-\mathcal{D}^{\mathsf{T}})\boldsymbol{\mu} = 0$ and $\boldsymbol{n}_0 \notin R(\frac{1}{2}+\mathcal{D}^{\mathsf{T}})$. So $\boldsymbol{n}_0$ has a component in $N(-\frac{1}{2}+\mathcal{D})$ and $(n_0, \boldsymbol{\xi}_0) \neq 0$.

Full-rank operators for bounded domains. From Proposition 1, we know the following facts: $\boldsymbol{n}^{\mathsf{T}}(-\frac{1}{2}+\mathcal{D}) = 0$ and $(-\frac{1}{2}+\mathcal{D})\boldsymbol{\xi} = 0$. Therefore, the Jordan block of eigenvalue 0 has size 1 and $(\boldsymbol{n}, \boldsymbol{\xi}) \neq 0$. Therefore, by using Wielandt's deflation, we construct an equivalent operator of full rank

$$\boldsymbol{u} = (-\frac{1}{2}+\mathcal{D}+\boldsymbol{n}\boldsymbol{n}^{\mathsf{T}})\boldsymbol{\mu}.$$

Full-rank operators for multiply connected domains. By Proposition 3, the Jordan block of eigenvalue 0 is of size 1. We know that $\boldsymbol{n}^{\mathsf{T}}(-\frac{1}{2}+\mathcal{D})=0$ and $(-\frac{1}{2}+\mathcal{D})\boldsymbol{\xi}_0=0$. Since $(\boldsymbol{n},\boldsymbol{\xi}_0)=(\boldsymbol{n}_0,\boldsymbol{\xi}_0)\neq 0$, the equivalent full-rank operator is

$$\boldsymbol{u}=(-\frac{1}{2}+\mathcal{D}+\boldsymbol{n}_0\boldsymbol{n}^{\mathsf{T}})\boldsymbol{\mu} \quad \text{or} \quad \boldsymbol{u}=(-\frac{1}{2}+\mathcal{D}+\boldsymbol{n}\boldsymbol{n}^{\mathsf{T}})\boldsymbol{\mu}$$

REFERENCES

[1] Milton Abramowitz and Irene A. Stegun. *Handbook of mathematical functions*. Dover Publications, 1964.

[2] Y. Achdou and Olivier Pironneau. A fast solver for Navier-Stokes equations in the laminar regime using mortar finite element and boundary element methods. *SIAM Journal on Numerical Analysis*, 32(4):985–1016, 1995.

[3] George Biros, Lexing Ying, and Denis Zorin. The embedded boundary integral method for the stokes equations. *Submitted for publication*, 2002. (For reviewers: `http://www.cs.nyu.edu/~biros/jcp-ebi-stokes.pdf`).

[4] Donna Calhoun. A Cartesian grid method for solving the two-dimensional streamfunction-vorticity equations in irregular regions. *Journal of Computational Physics*, 176:231–275, 2002.

[5] Jim Douglas Jr. and Thomas F. Russell. Numerical methods for convection-dominated diffusion problems based on combining the method of characteristics with finite element or finite difference procedures. *SIAM Journal on Numerical Analysis*, 19(5):871–885, 1982.

[6] Leslie Greengard and Mary Catherine Kropinski. An integral equation approach to the incompressible Navier-Stokes equations in two dimensions. *SIAM Journal on Scientific Computing*, 20(1):318–336, 1998.

[7] Leslie Greengard and Vladimir Rokhlin. A fast algorithm for particle simulations. *Journal of Computational Physics*, 73:325–348, 1987.

[8] Morton E. Gurtin. *An Introduction to Continuum Mechanics*. Academic Press, 1981.

[9] Sharad Kapur and Vladimir Rokhlin. High-order corrected trapezoidal quadrature rules for singular functions. *SIAM Journal on Numerical Analysis*, 34(4):1331–1356, 1997.

[10] Sangtae Kim and Sappo J. Karrila. *Microhydrodynamics: Principles and Selected Applications*. Butterworth-Heinemann, 1991.

[11] Alex Klawonn. *Preconditioners for Indefinite Systems*. PhD thesis, Courant Institute, New York University, New York, NY 10021, 1996.

[12] Rainer Kress. *Linear Integral Equations*. Applied Mathematical Sciences. Springer, 1999.

[13] Ming-Chih Lai and Charles Peskin. An Immersed Boundary Method with formal second-order accuracy and reduced numerical viscosity. *Journal of Computational Physics*, 160:705–719, 2000.

[14] Zhilin Li and Ming-Chih Lai. The immersed interface method for the Navier-Stokes equations with singular forces. *Journal of Computational Physics*, 171:822–842, 2001.

[15] Anita Mayo. The fast solution of Poisson's and the biharmonic equations on irregular regions. *SIAM Journal on Numerical Analysis*, 21(2):285–299, 1984.

[16] Sean Norburn and David Silvester. Fourier analysis of stabilized Q1-Q1 mixed finite element approximation. Numerical Analysis Report 348, The University of Manchester, 1999.

[17] Olivier Pironneau. On the transport-diffusion algorithm and its applications to the Navier-Stokes eqautions. *Numerische Mathematik*, 38:309–332, 1982.

[18] P. Ploumhans, G.S. Winchkelmans, John K. Salmon, Anthony Leonard, and M.S. Warren. Vortex method for direct numerical simulation of three-dimensional bluff body flows: Application to the sphere at Re=300, 500, and 1000. *Journal of Computational Physics*, 178:427–463, 2002.

[19] Henry Power and L. Wrobel. *Boundary Integral Methods in Fluid Mechanics*. Computational Mechanics Publications, 1995.

[20] Andrew Staniforth and Jean Côté. Semi-Lagrangian integration schemes for atmospheric models—a review. *Monthly Weather Review*, 119:2206–2223, March 1991.

[21] John Strain. Locally-corrected multidimensional quadrature rules for singular functions. *SIAM Journal on Scientific Computing*, 6(4):992–1017, 1995.

[22] Dongbin Xiu and George Em Karniadakis. A semi-Lagrangian high-order method for Navier-Stokes equations. *Journal of Computational Physics*, 172(2):658–684, 2001.